RSC Advances

Tubeless biochip for chemical stimulation of cells in closed-bioreactors: anti-cancer activity of the catechin-dextrane conjugate

5   Sandro Meucci[ab], Marco Travagliati[ab], Orazio Vittorio[a], Giuseppe Cirillo[cd], Luca Masini[ab], Valerio Voliani[ab], Nevio Picci[c], Fabio Beltram[ab], Alessandro Tredicucci[a] and Marco Cecchini[a]

[a] NEST, Scuola Normale Superiore and Istituto Nanoscienze-CNR, Piazza San Silvestro 12, Pisa 56127, Italy

10

[b] Center for Nanotechnology Innovation @ NEST, Istituto Italiano di Tecnologia, Piazza San Silvestro 12, Pisa 56127, Italy

[c] Department of Pharmacy, Health and Nutritional Sciences, University of Calabria, I-87036 Rende (CS), Italy.

15

[d] Leibniz Institute for Solid State and Materials Research Dresden, D-01171 Dresden Germany.

* e-mail: marco.cecchini@nano.cnr.it

20

Keywords: microfluidic, tubeless, bubble-free, pharmacokinetics, microchamber, chemical gradient

Abstract

The most exciting promise of cell micro-bioreactors is their expected ability to reproduce specific aspects of physiological environments *in vitro*, singularly or in combination, and to perform

25   advanced biological studies to unravel novel interaction mechanisms; but this challenge is formidable. Moreover, the use of microfluidics is limited by the difficulty to adapt standard tissue culture protocols to miniaturised biochips and by the need of bulky external equipment such as liquid pumping systems. Here, we introduce an original microfluidic gradient generator for culturing cells in closed microchambers, based on: 1. automatic cell valving, 2. hydrostatic-pressure

30   pumping, and 3. *on-chip* liquid reservoirs. The biochip is designed to be fully compatible with standard biological procedures and to operate with no external control units or cumbersome ancillary components. Remarkably, the use of integrated liquid reservoirs prevents air bubble formation and associated channel clogging. We detail the rationale behind the fluidic design, simulate and measure the chip fluid-dynamics by finite element simulations and microflow

35   velocimetry, respectively. We finally exploit our chip to study the kinetics of an anti-cancer

molecule, the catechin-dextran conjugate, on HeLa cells, demonstrating a very fast action. We argue that the presented fluidic concept and architecture are not limited to the present realization, but can be easily applied to other chip geometries and adapted to a number of biological studies.

1 Introduction

40   Cells are exposed to a plethora of physico-chemical stimuli that regulate their functional response and the overall physiology of their host tissue. Cell-cell contact and long-distance interactions [1–3], local cross-talk with extracellular matrix domains [4, 5] are but few examples of the complexity of signalling that we find in a living organism. The ability to reproduce specific aspects of this

45   environment in artificial devices *in vitro*, would make it possible to dissect their individual interplay with other stimuli and would bring to a new level our ability to investigate biological processes, but the challenge is formidable.

The field of microfluidics has brought great improvements in this direction, allowing for the fine control over the local chemistry [6, 7] and physics [8, 9] of extracellular environment *in vitro*.

50   A particular effort was directed to shaping chemical gradients in microsized cell bioreactors. This was achieved by exploiting some characteristics of the microfluidic regime, such as the laminar flow [10, 11]. A number of biodevices were proposed to study relevant cell biology aspects, such as cell migration [12, 13], axon guidance [14] and stem cell differentiation [15].

Although devices such as these did show great potential, several drawbacks have limited

55   their widespread use in cell biology. Indeed they typically require complex fabrication processes, bulky external pressurization systems for valve and liquid actuation [16] that are normally connected to the microchip by fixed tubing. Additionally, dedicated skilled operators are necessary to run such experiments. Recently, a few alternative ways to actuate and control flows in micro-environments were proposed, using cells themselves to drive liquid routing [17, 18] and open

60   chambers to facilitate cell loading and medium exchange [19, 20].

Here, we introduce an original microfluidic gradient generator for culturing cells in closed microchambers that is compatible with standard biological procedures and does not require external control units and tubing. A reduction of dead volume is obtained, as well as simplified cell loading and culturing. Liquid reservoirs are embedded in the fluidic layer of the device, allowing liquids to

65   quickly reach thermal equilibrium with the chip. This configuration minimizes the presence of

temperature gradients, and avoids air bubble nucleation, one of the major issues of microfluidic devices. We applied the present chip to the study of the anti-cancer properties of catechin-dextran conjugate (CT-Dex). Catechin (CT) is a widely studied natural active ingredient found in many natural matrices, including green tea, and is widely recognized as co-adjuvant in cancer therapy [21,

70   22]. CT conjugation with dextran leads to improved CT stability while maintaining anti-cancer activity *in vitro* [23]. To date no data are yet available on its kinetics. By exploiting the unique fluidic control provided by our chip, we cultured cancer cells and applied a spatially modulated CT-Dex treatment. Cancer cell death dynamics was followed and quantitatively evaluated using fluorescent dyes and time-lapse microscopy.

75

2 Results and Discussion

2.1 Chip design and fluid dynamic characterization

The device presented here was designed to allow efficient cell loading and long-term culture in closed microchambers. Importantly it requires only the typical equipment found in a tissue culture laboratory, while yielding fine control over fluid dynamics in the cell-culture area.

A schematic view of the chip design is shown in Fig. 1 (see also Sec. 3.1 for details). The fluidic network is composed by a central 7.5 nL microchamber (MC, 500 μm x 500 μm x 30 μm), from which three channels depart in a *T-shaped* geometry. These channels connect the MC to open liquid reservoirs (LRs), which can be filled by standard pipetting with 450 μL of liquid (Supp. Fig. 1), providing a hydrostatic pressure of 150 Pa (Eq. 1, Sec. 3.1). Two sets of 2.5 x 10 μm^2 parallel microchannels are located between the MC and the two lateral channels (Fig. 1d) acting as filters for suspended microparticles and, during cell loading, as barriers for suspended cells (see Sec. 3.2). For this reason, in the following they will be called filter channels (FCs). Their hydraulic resistance is much greater than the other microchannels (Tab. 1) so that more than the 90% of the total pressure drop is located at their ends. As a consequence, morphological imperfections of the fluidic accesses or along the large-section microchannels marginally affect the pressure values at the three open sides of the MC and its fluid dynamics. The chip hydraulic resistance was dimensioned in order to have a fast liquid turnover in the MC while minimizing the flow rate and, consequently, the shear stress applied to the cells. This point is crucial, since high flow rates lead to rapid equilibration of the liquid levels in the reservoirs and to the end of the perfusion. Owing to the FC high resistance, however, the maximum flow rate achievable using the hydrostatic pressure provided by the reservoirs is limited to 2.5 nL/s. Given the large volume of the reservoirs (450 μL) the pressure drop is reduced only by the 2 % per hour of chip operation (Supp. Fig. 2). Nevertheless, this flow rate corresponds to a turnover time of the liquid in the MC of 3 s, assuring a fast delivery of fresh nutrients to the cells and washout of metabolic wastes.

The fluidic behaviour in the MC is determined by the balance of the flows through the lateral channels (*perfusion channels*) and the central one (*waste/loading channel*) (Fig. 1d), and can be described by defining the two pressure differences ΔP_D and ΔP_S as described in Eq. 2 in Sec. 3.1.

105   The sign of ΔP_D determines the flow direction in the central channel. For positive values the liquid flows from LR_C to the MC, passes through the FCs and reaches LR_A and/or LR_B; in the following we will refer to this case as *loading mode* (Fig. 1c). For negative values ($\Delta P_D < 0$) the flow direction is inverted, and the liquid enters into the MC from one or both the perfusion channels, and reaches LR_C. This operating mode will be called *perfusion mode*. The balance between flows in the

110   perfusion channels is regulated by ΔP_S (Fig. 1c and 2): the flow is symmetric if this variable is equal to zero and spatially biased otherwise.

In order to assess device performance in creating and controlling different fluidic configurations, several combinations of ΔP_D and ΔP_S were simulated by finite element method analysis and experimentally characterized by spatio-temporal image correlation spectroscopy

115   (STICS) [24] (see Sec. 3.3 and Sec. 3.4). Data reported in Fig. 2 demonstrate that the hydrostatic pressure alone can finely control the microfluidic device, and that all measurements agree remarkably well with data obtained *in silico*. As expected, laminar flow dominates the fluid dynamics in the MC (Reynolds number Re = 8e-4 ≪ 1, Peclet number Pe = 10 ≫ 1). As a consequence, opposite parts of the MC can be chemically decoupled by operating in perfusion

120   mode. This is achieved if the diffusion of the solute molecules is slow compared to the fluid velocity in the MC. For example, in the case of a small molecule in water (*e.g.* glucose, diffusion coefficient $D_g = 600\ \mu m^2/s$), the time required for complete diffusion within the MC is of the order of 104 s, a value much greater than the typical fluid turnover time (7.5 s for a slow rate of 1 nL/s). The velocity field in the MC (Fig. 2a) is used to calculate the shear stress experienced by cells.

125   According to Eq. 5, the maximum spatially-averaged value, obtained for $\Delta P_D = 150$ Pa, is 8.3 ± 0.4 mPa. Yet, 90% of the MC area return shear stress values lower than 15 mPa (Fig. 2d).

An increasing number of studies are proposing hydrostatic-pressure-driven microfluidic

devices for implementing cell cultures at the microscale [25–27], but this pumping methods has few disadvantages that must be taken into account. In particular, the maximum flow rates that can be achieved are limited by the reservoir capacities and a dynamic control of the flows requires to add or remove liquids from the reservoirs. For our geometrical design, a strategy to overcome these issues is to directly connect the liquid reservoirs with pressurized-air lines. Since no liquids are injected into the chip, the thermal equilibrium of the reservoirs with the chip is not compromised and dead volumes are not increased. Moreover, air-to-liquid interfaces are easily connected/disconnected without the risk of trapping air bubbles in the fluidic network. The graph in Fig. 3 shows the average velocity measured in the MC as a function of the external pressure applied to LR_C. The first part of the curve ($\Delta P_D \leq 1600$ Pa) shows a linear trend compatible with a pure resistive behaviour. At steady state the pressure-driven flow is regulated by $q = \Delta P/R$, where q is the flow rate and ΔP is the pressure drop. Since q is proportional to the average velocity (v) in the channel: $v/\Delta P = \alpha$ where α is the slope of the speed/pressure curve. The slope of the linear fit calculated for $1 \leq \Delta P \leq 1600$ Pa (red line in Fig. 3) is 5.35e-2±0.74e-2 µm/s Pa, in agreement with simulations (5.28e-2 µm/s Pa). For higher pressure values the average measured speed saturates. This behaviour suggests the presence of pressure leaks that probably stem from a non-optimal sealing between the external tubing and the LRs.

2.2 Cell loading and cytocompatibility experiments

During typical operation the whole chip (reservoirs included) is maintained within an incubator (T = 37 °C, 5% CO_2) in thermal equilibrium with the external environment. In this condition, on-chip liquid reservoirs lead to a reduction of dead volumes, efficient gaseous and thermal equilibration between the chip and the environment. This minimizes the presence of temperature and gas-liquid solubility gradients along the liquid paths, resulting in negligible air bubble nucleation and microchannel clogging. Gas bubble formation is a very limiting factor in microfluidic devices and the published approaches to address this issue focused on removing bubbles already present in the chip by using dedicated elements such as hydrophobic paths to create

gas-liquid interfaces on-chip [28], bypass channels to collect and drive air bubbles off-chip [29] or
155   vacuum lines for gas removal [30, 31]. However, the integration of bubble trappers increases device-manufacturing and operation complexity. Here, the prevention of gas bubbles nucleation in the microchannels is obtained localizing the liquid-to-air interface *on chip*. To this end, open liquid reservoirs and an on-chip pneumatic pressurization system were implemented.

Cell loading is obtained by exploiting the difference in cross-sections between the FCs and
160   the rest of the channels (Tab. 1). Since suspended cells typically have a circular cross-section with an average diameter of 10 μm, they cannot pass through the thin FCs (2.5 μm x 10 μm) which act as barriers, leading to cell accumulation at their ends.

The loading procedure can therefore be divided into three phases: 1. $LR_{A,B}$ are emptied and LR_C is filled with the cell suspension as schematized in Fig. 4a; 2. flow is activated by gravity from
165   LR_C down to the MC (Fig. 4b), cells move into the MC by viscous drag and progressively accumulate at FCs entrances (Fig. 4c); finally 3. when all FCs are occluded by cells, the flow automatically stops, thus preventing an excessive cell density to build up. Cells adhere and spread on the MC bottom layer in approximately 30 min and liquid flow is restored. After cell spreading LR_A and LR_B are filled with standard cell culture medium in order to obtain flow inversion, *i.e.*
170   fluids move from $LR_{A,B}$ down to the MC and reach LR_C. The use of FCs allows a reduction of cell-suspension density with respect to those typically required by standard loading methods [9, 18, 27]. Moreover, cells localize only in the active part of the device (*i.e.* the MC), thus avoiding possible chemical interactions with cell colonies developing in other parts of the microfluidic chip. This effect is known as cellular valving and was also implemented by other groups for single-cell
175   positioning in microchannels [17, 18]. Our chip yields for the first time cellular valving as an automated process for cell loading and for controlling cell density in the culture area, operations that typically require pneumatic soft valves and complex chip geometries [32–35].

After cell-loading, liquid reservoirs are accessible to deliver substances (*e.g.* drugs, growth factors, etc.) into the MC via the perfusion channels, according to the specific experimental protocol

180   (examples are described in Sec. 2.3). The above described loading protocol was tested with different cellular models – human cervical carcinoma cell line (HeLa), rat embryonic fibroblasts (REF) and human embryonic kidney cells (HEK) – using the same culturing protocols and no important differences were observed in chamber filling and colonization.

185   The biocompatibility of the microfluidic device was demonstrated by loading HeLa cells in the MC as described in Sec. 3.6 and monitoring their growth over days. Bright-field images of the developing cell colonies were acquired every 12 h. A vitality test was performed after 72 h in culture, adding Calcein AM [36] in the perfusion medium (Sec. 3.6) to stain living cells under constant flow. The colonization of the MC (Fig. 4c) is characterized by a first phase where suspended cells adhere and spread, occupying the area close to the CFs and a second one in which
190   they start replicating and reach confluence with a density of about 6e4 cells/cm^2. This behaviour is quantified in Fig. 4d where the number of cells is reported vs. time during symmetric perfusion. An initial lag of 24 h precedes a regular growth curve, in agreement with what observed in similar conditions by other groups [37–39]. The cultures show a growth rate of 0.023±0.002 h^{-1} and a viability, calculated as the percentage of Calcein AM-positive cells, at 72 h of 88%±3% (Calcein
195   AM, Sec. 3.6). These values are in line with those measured in standard culture conditions by us (0.028±0.007 h^{-1}) and by other groups (*i.e.* 0.025 h^{-1} on average in multiwell plates [40]). They also are very similar to those measured in other published microfluidic devices under similar flow conditions [38, 39]. The time required to reach confluence depends on the initial cell density and can be reduced using more concentrated cell-suspensions during the loading phase. In order to
200   measure the doubling time, the initial cell density was chosen to reach confluence in long terms (>72 h), allowing a more accurate calculation of the growth rate. Cells did duplicate and showed a healthy morphology, demonstrating that the nutrients provided by the perfusion and the washout of the waste was sufficient for reaching and maintaining confluence. Finally, we also stress that shear stress did not reduce cell viability and growth.

2.3 Chemical gradient generation and CT-Dex-induced cell death

Owing to the characteristics of laminar flow, the gravity-driven operating mode can be successfully exploited to chemically de-couple opposite sides of the MC, and to form chemical gradients whose spatial profiles are determined by ΔP_S and ΔP_D. In order to demonstrate an experimental application, we performed a pharmacokinetics study of CT-Dex. CT-Dex was synthesized by employing the optimized conditions reported in [23]. Cancer cells (HeLa) were loaded into the biochip and cultured to confluence under symmetric perfusion. CT-Dex was then delivered from one of the PCs. Symmetric perfusion was maintained for the whole experiment, leading to the formation of a stable and symmetrical CT-Dex gradient within the MC. This gradient formation technique is similar to the one of the microfluidic jet device (µFJ) reported in [41], but this last device is based on open chambers and no flow can be activated in the microchamber.

In order to better characterize the spatial distribution of drug concentration, a preliminary experiment was carried out with a fluorescently-labeled variant of the drug, obtained by substituting the CT with fluorescein with the same stoichiometric ratio. This substitution does not alter the diffusion properties of the compound, since fluorescein is very similar in weight and charge to CT (332.31 and 290.27 Da, respectively) and both of them are much smaller than the Dex (5 kDa). The dye (150 µg/mL in DMEM) was administrated from the left and DMEM from the right perfusion channel. Figure 5a shows an epifluorescence image of the MC area where the bright and dark regions are associated with high and low concentration levels of labeled-Dex, respectively. Remarkably, $\Delta P_S = 0$ Pa led to the transition region being placed at the center of the MC and $\Delta P_D = 150$ Pa led to a very steep concentration gradient. Specifically, the spatial extent of the concentration gradient was limited to $75\,\mu$m, in very good agreement with the FEM simulations (Fig. 5b), demonstrating that the two sides of the MC are chemically decoupled.

Other devices, like the ones presented by Taylor *et al.* [42] and Pyerin *et al.* [43] were based on subcellular-sized channels for creating compartmentalised cultures that could be chemically isolated by hydrostatic pressure. However, this architecture is based on the physical separation of

the two culture chambers and allows neither for perfusion of the cell cultures, nor for chemical gradient generation. Instead, continuous perfusion devices such as the T-sensor [44] could exploit the slow diffusion typical of laminar flow to create chemical gradients at the meeting point of converging microchannels. Kunze *et al.* [27] proposed a device where the cells were cultured in two chambers separated by a connecting channel. A linear gradient was generated in this channel by loading two different solutions in the culture chambers, but the equilibration time of the reservoirs was limited to 75 min. Our chip combines the advantages provided by these two technologies in a versatile and easy-to-use tool for continuous perfusion bioreactors. As previously mentioned, HeLa cells were loaded into the device and left to grow until confluence. Calcein AM was then administrated from both perfusion channels to stain viable cells; then, CT-Dex (150 μg/mL in DMEM) was introduced from the left perfusion channel. The fluorescence signal was monitored by time-lapse microscopy for 5 h (Fig. 5c). Cells were not affected by CT-Dex during the first two hours of treatment. Then intense blebbing affected the cells close to the CT-Dex administration area (Supp. Fig. 3) and fluorescence started to decrease, indicating progressive cell death. The wave of cell death propagated toward the centre of the chamber, reducing the integrated Calcein AM fluorescence signal in the treated area down to below 10% after 260 min of treatment (Fig. 5d). Conversely, non-treated cells (right side of the MC, Fig. 5a) showed a stable Calcein AM signal throughout the experiment (Fig. 5c), indicating that laminar flow was not significantly affected by the presence of the cells. Moreover, this demonstrates the efficacy of the drug anti-cancer activity, and that cell viability was not reduced by possible cross talk with the neighbour dying cells. To the best of our knowledge, this is the first example of a bio-chip where the dynamics of drug-induced death in cancer cells was studied. Previous reports present chips mainly based on cyclic voltammetry and commercial drugs such as Etoposide, Placlitaxel, Hydroxyurea, Cyclophosphamide, *etc* [45–48] were used. In these papers, a good anticancer activity (reduction of the cell viability by 50%) was recorded only after 12 h (for etoposide and Placlitaxel) or 24 h (for Hydroxyurea and Cyclophosphamide) incubation times. Our data report a reduction of cell viability

to about 10% after only 260 min, indicating that CT-Dex can rapidly interact with and kill HeLa

cancer cells.

3 Materials and methods

3.1 Chip architecture and modeling

The device is composed of channels of varying thicknesses. The *thick* ones (30 µm) include the culture chamber and the three channels connected to the LRs (Fig. 1). These channels consist of two symmetrical perfusion channels which connect to $LR_{A,B}$ and the central one connecting to LR_C. The *thin* FCs are 2.5 µm thick, grouped in two sets of 25, and are located on either side of the MC (Fig. 1). The geometry of each fluidic element is reported in Tab. 1.

	(L x w) [µm]	Thickness [µm]	Cross-section [µm^2]	Hydraulic resistance [mBar s / nL]
Perfusion channels	3000 x 150	30	4500	10.19e-2
Waste/loading channel	2000 x 200	30	6000	4.92e-2
Filter channel	100 x 10	2.5	25	91.34

Table 1: Channel geometrical characteristics and hydraulic resistance.

The inlet pressure is calculated by:

$$P_i = \rho g h_i \qquad\qquad 1$$

where *h* is the height of the liquid column at the *i*-th reservoir, *g* is the gravitational acceleration and ρ is the liquid density. For the case of diluted aqueous solutions $\rho \approx \rho_{H_2O} = 10^3 kg/m^3$. Given the symmetry of the device, two pressure differences ΔP_S and ΔP_D can be defined to describe the fluid-dynamics in the MC:

$$\begin{cases} \Delta P_S = P_A - P_B \\ \Delta P_D = P_C - \frac{P_A + P_B}{2} \end{cases} \qquad\qquad 2$$

where P_A, P_B and P_C are the pressures at inlets A, B and C, respectively. ΔP_S and ΔP_D determine the flow rates along the branches A, B and C ($q_{A,B,C}$):

$$\begin{cases} q_A = \frac{1}{2R}\Delta P_S - \frac{1}{R+2R_C}\Delta P_D \\ q_B = -\frac{1}{2R}\Delta P_S - \frac{1}{R+2R_C}\Delta P_D \\ q_C = \frac{2}{R+2R_C}\Delta P_D \end{cases} \qquad 3$$

Here, R_C and R are the hydraulic resistances between the MC and LR_C and $LR_{A,B}$, respectively. The hydraulic resistances of the microchannel network were chosen so that fluids could be actuated using the hydrostatic pressure provided by the reservoir liquids. The hydraulic resistance R of a rectangular microchannel is given by:

$$R = \frac{12\eta L}{1-0.63(h/w)}\frac{1}{h^3 w} \qquad 4$$

where η, L, h and w are the liquid viscosity, channel length, height and width, respectively [49]. Equation 4 was used to calculate R for each fluidic element and to model the microfluidic chip as a simplified equivalent fluidic circuit (Supp. Fig. 4).

3.2 Chip fabrication

A textured SU8 on silicon substrate was fabricated as a master mold. A layer of SU8 2002 (2.5 μm thick) was spin-coated onto a silicon wafer and exposed by electron beam lithography to define the FCs. Then, a second layer of SU8 2025 was spin-coated to obtain a total thickness of 30 μm and exposed by photolithography to create the culture chamber and the inlet/outlet channels. The two expositions were developed in a single step for 2.5 min in SU8 developer (Allresist GmbH). Finally, the mold was hardbaked at 200 °C for 20 min and treated with trimethylchlorosilane vapour (Sigma Aldrich) for 10 min to ease the master-replica detachment.

The fluidic layer was fabricated by a single step PDMS replica moulding process. To create the accesses between the reservoirs and the fluidic layer, 2 mm holes were punched using a Harris Uni-Core 2 mm puncher. PDMS replicas were then attached to cyclic olefin copolymer (COC) foils (IBIDI; Martinsried, Germany), a transparent material whose biocompatibility has been assessed in previous studies [50–55]. A heterogeneous bonding protocol was used to obtain an irreversible bonding between COC and PDMS, as reported in [56]: replicas and COC foils were exposed to

oxygen plasma (1.4e-1 mBar, 10 W) for 25 s and 15 s, respectively. PDMS and COC were then immersed in a 1% aminopropyltriethoxysilane (APTES) aqueous solution and in water, respectively. After 20 min, the substrates were carefully dried with nitrogen flow and brought into conformal contact at room temperature. An irreversible bond formed after approximately one hour.

305 Finally, the liquid reservoirs were attached to the chips (Fig. 1a) with silicon glue (RS Components RS692-524). Hollowed, threaded cylinder vials with 4 mm internal diameter and 200 μL capacity were chosen as reservoirs.

3.3 Finite-element-method (FEM) simulations

Three-dimensional computation fluid dynamics (CFD) investigations were performed on the MC

310 using finite element method simulations (COMSOL Multiphysics 4.2).

The stationary velocity field inside the microstructure was obtained by solving the Navier-Stokes equation for an incompressible fluid in the laminar flow regime assuming no-slip condition everywhere except on the surfaces connecting to the $LR_{A,B,C}$ where the pressure value was fixed and inlet or outlet boundary conditions were applied. Pressure values on these boundaries were modified

315 parametrically via a Java script.

Diffusion of CT-Dex in the selected velocity fields was calculated assuming $T = 37\,°C$ and integrating Fick's law on the same mesh used for the velocity field calculation (CT-Dex diffusion coefficient $D = 6e\text{-}11\ m^2/s$ [57].

3.4 Microflow velocimetry and shear stress calculation

320 Velocity fields inside the MC were measured via STICS using a standard inverted microscope (Nikon Eclipse Ti) equipped with a fast camera (Basler A602-f). The device was filled with a suspension of 500 nm latex beads (Sigma-Aldrich L3280 diluted 1:10 in water) and a time series of 300 bright-field micrographs of the entire microchamber was acquired at 30 fps with an air 10x NA = 0.45 objective and a 1.5x lens (1.07 μm/pixel).

325 Active pressurisation measurements (Sec. 2.1) were performed after seeding the fluid with 100 nm

particles (Sigma-Aldrich L9902). In order to further reduce microchannel clogging at these high

flow rates, the suspension (diluted 1:5 in water) was filtered using a membrane with 0.22 μm pores

(Millipore Millex-GP Filter unit) prior to experiments. A 6000 frame time series was acquired in

bright-field microscopy at 400 fps with an air 20x NA = 0.45 objective and a 1.5x lens

330　(0.53 μm/pixel). Calculations were carried out in the hydrostatic regime on a square grid of points

separated by a = 8 μm using 16 μm-wide interrogation areas, while for the active pressurization

measures both the pitch of the grid and the size of the interrogation areas were increased to 30 μm

to increase the signal-to-noise ratio. Further details about STIC velocimetry in microfluidics are

reported in [24, 58].

335　The shear stress experienced by cells in the MC was calculated by assuming that the fluid velocity

field near the substrate (0 < z < 2.5 μm, where z is the vertical distance from the MC bottom layer)

varied linearly with z. Simulations (Supp. Fig. 5) showed that this hypothesis leads to a good

approximation of the actual velocity profile (error < 1%). Shear stress is thus calculated by

$$\tau = \mu \frac{\partial u}{\partial z} ,$$

5

340　where μ is the dynamic viscosity of the liquid, u(z) is the average velocity measured in the chamber

as a function of z.

3.5 Microchannel filling and cell-loading protocol

A reproducible and reliable filling of the microfluidic network was obtained by degasing the whole

chip at $4e^{-2}$ mBar for 10 min, sterilized by oxygen plasma treatment (60 s, $1.4e^{-1}$ mBar, 10 W) just

345　before LR filling and immediately moved into the incubator (37 °C, 95% humidity, 5% CO_2). The

absorption of air into degased PDMS was used to fill the channels as described in [59] and, at the

same time, it prevented bubble formation during the heating of the device. The whole process was

achieved in approximately 20 min.

Before cell loading the chips were filled with DMEM, and incubated for 1 h. Cells were harvested

350　and diluted at a concentration of $3e^5$ cells/mL. In order to obtain symmetric cell loading, the

reservoirs were emptied and 450 μL of cell suspension was added into LR_C (Fig. 4). After 30 min, LR_C was emptied and perfusion was restored by adding 450 μL of fresh DMEM into $LR_{A,B}$.

3.6 Cell-viability experiments

HeLa cells were obtained from American Type Culture Collection (ATCC, Rockville, Maryland).

355   HeLa cells were grown in a complete culture medium consisting of DMEM supplemented with 2 mM L-glutamine, 100 IU/mL penicillin, 100 μg/mL streptomycin, and 10% heat-inactivated fetal bovine serum (Gibco, Invitrogen). Cells were detached by trypsinization, counted in a Thoma's camera and suspended in cell culture medium at a concentration of $3x10^5$ cells/mL.

Cell vitality was measured by Calcein AM assay after 72 h in culture. HeLa cells were injected in

360   the system and left to adhere in the MC. Cells were stained with 2 M calcein-AM solution (Molecular Probe, Eugene, OR, USA) at room temperature for 30 min according to the manufacturer's protocol. Calcein AM is a cell-permeant dye that can be used to determine cell viability in most eukaryotic cells. In living cells the non-fluorescent calcein AM is converted to green-fluorescent calcein (ex/em 495/515 nm) after acetoxymethyl ester hydrolysis by intracellular

365   esterase, resulting in a staining of living cells only. Cell vitality was measured as the percentage of Calcein AM positive cells in the MC.

HeLa cells growth rate was measured in the MC in standard culture condition (ΔP_D = -150 Pa, ΔP_S = 0 Pa) by time-lapse bright field microscopy (Nikon Eclipse Ti). The cell doubling time was compared with that of cells cultured on standard culture dishes. Growth rate (μ) was calculated

370   from the exponential fit of the cell density (c) in the MC over time (Fig. 4).

$$c(t) = c_0 e^{\mu t} \qquad\qquad 6$$

where c_0 is the initial cell density and t is the time after cell loading.

3.7 CT-Dex experiments

HeLa cells were loaded as described in Sec. 3.5 and grown in the MC up to confluency. These

375   operations were performed in an incubated environment (37 °C, 95% humidity, 5% CO_2). After 6 h, living cells were stained with Calcein AM by delivering the staining solution (1 μL/mL in no serum

DMEM) from the perfusion channels for 20 min. Bright-field and fluorescence images of the cell culture were acquired every 5 min for 5 h with a Nikon-Ti PSF wide-field microscope (Nikon, Japan). A baseline (30 min) was acquired in order to determine photobleaching in the experimental

380 conditions used, then the staining solution was removed and 450 μL of CT-Dex (150 μg/mL in DMEM) and DMEM were loaded in the LR_A and LR_B, respectively.

The MC was divided into three adjacent regions of 166 μm x 500 μm, corresponding to different CT-Dex concentration regions (named *treated*, *gradient* and *untreated*) from the drug injection point to the opposite side of the MC respectively (Fig. 5a). For each time point, the fluorescence

385 signal in *treated* and *untreated* regions was integrated, corrected for the photobleaching and normalized to the initial value. Image analysis and signal normalization was performed using custom Matlab scripts.

4 Conclusions

390   We designed a tubeless microfluidic device that is able to yield long-term cell culturing and chemical-gradient shaping with no need of external pressure systems. Our device exploits the careful dimensioning of the hydraulic impedances to achieve precise control over fluid dynamics in closed MCs and uses the pressure of liquid columns in open LRs as driving force. This approach requires no ancillary equipment for operation and therefore can be readily used in standard tissue

395   culture laboratories. The open LRs also allow for a fast and efficient thermal and gaseous equilibration of the liquids with the chip, providing an efficient way to prevent gas bubble nucleation inside microchannels. A self-limiting automated cell loading protocol exploiting sub-cell-cross-section channels was successfully developed, leading to the fast and reproducible filling of the MC with cell suspensions. This protocol is based on the concept of cell valving and yields a

400   feedback-controlled loading that allows a correct handling of the device even by unskilled operators. Finally, we performed an assay to study the kinetics of an anti-cancer molecule, the CT-Dex conjugate, on HeLa cells. We demonstrated rather fast action compared to data obtained with other commercial drugs (*i.e.* etoposide, Placlitaxel, Hydroxyurea and Cyclophosphamide).

The fluidic concept described and demonstrated here is not limited to the present realization, but

405   can be rather straightforwardly applied to other chip geometries and adapted to other biological studies.

5 Acknowledgments

References

[1] M. Sampaolesi, S. Janssens, Cardiovasc. Res., 100 (2013) 178–80.

[2] C.C. DuFort, M.J. Paszek, V.M. Weaver, Nat. Rev. Mol. Cell Biol., 12 (2011) 308–319.

[3] L.A. Lowery, D. Van Vactor, Nat. Rev. Mol. Cell Biol., 10 (2009) 332–343.

[4] B. Geiger, J.P. Spatz, A.D. Bershadsky, Nat. Rev. Mol. Cell Biol., 10 (2009) 21–33.

[5] M.C. Dodla, R. V Bellamkonda, Biomaterials, 29 (2008) 33–46.

[6] B.G. Chung, F. Lin, N.L. Jeon, Lab Chip, 6 (2006) 764–8.

[7] R. Sahai, C. Martino, P. Castrataro, A. Menciassi, A. Ferrari, F. Beltram, M. Cecchini, Microelectron. Eng., 88 (2011) 1689–1692.

[8] S. Han, K. Yang, Y. Shin, J.S. Lee, R.D. Kamm, S. Chung, S.-W. Cho, Lab Chip, 12 (2012) 2305–8.

[9] L.L. Bischel, E.W.K. Young, B.R. Mader, D.J. Beebe, Biomaterials, 34 (2013) 1471–7.

[10] N.L. Jeon, S.K.W. Dertinger, D.T. Chiu, I.S. Choi, A.D. Stroock, G.M. Whitesides, Langmuir, (2000) 8311–8316.

[11] D. Irimia, D. a Geba, M. Toner, Anal. Chem., 78 (2006) 3472–3477.

[12] R. Sahai, M. Cecchini, M. Klingauf, A. Ferrari, C. Martino, P. Castrataro, V. Lionetti, A. Menciassi, F. Beltram, Microfluid. Nanofluidics, 11 (2011) 763–771.

[13] N. Li Jeon, H. Baskaran, S.K.W. Dertinger, G.M. Whitesides, L. Van de Water, M. Toner, Nat. Biotechnol., 20 (2002) 826–30.

[14] R. Xiao, W. Zeng, Y. Li, W. Zou, L. Wang, X. Pei, M. Xie, W. Huang, (2013).

[15] J. Kawada, H. Kimura, H. Akutsu, Y. Sakai, T. Fujii, Lab Chip, 12 (2012) 4508–4515.

[16] M.A. Unger, H.P. Chou, T. Thorsen, A. Scherer, S.R. Quake, Science, 288 (2000) 113–6.

[17] J.-P. Frimat, M. Becker, Y.-Y. Chiang, U. Marggraf, D. Janasek, J.G. Hengstler, J. Franzke, J. West, Lab Chip, 11 (2011) 231–7.

[18] N.-D. Dinh, Y.-Y. Chiang, H. Hardelauf, J. Baumann, E. Jackson, S. Waide, J. Sisnaiske, J.-P. Frimat, C. Van Thriel, D. Janasek, J.-M. Peyrin, J. West, Lab Chip, 13 (2013) 1402–12.

[19] N. Bhattacharjee, N. Li, T.M. Keenan, A. Folch, Integr. Biol. (Camb)., 2 (2010) 669–79.

[20] M. Hamon, S. Jambovane, L. Bradley, A. Khademhosseini, J.W. Hong, Anal. Chem., 85 (2013) 5249–5254.

[21] I. Bosma, J.C. Reijneveld, L. Douw, M.J. Vos, T.J. Postma, N.K. Aaronson, M. Muller, W.P. Vandertop, B.J. Slotman, M.J.B. Taphoorn, J.J. Heimans, M. Klein, Neuro. Oncol., 11 (2009) 51–8.

[22] R. Zhou, R. Mazurchuk, R.M. Straubinger, Cancer Res., 62 (2002) 2561–6.

[23] O. Vittorio, G. Cirillo, F. Iemma, G. Di Turi, E. Jacchetti, M. Curcio, S. Barbuti, N. Funel, O.I. Parisi, F. Puoci, N. Picci, Pharm. Res., 29 (2012) 2601–14.

[24] M. Travagliati, S. Girardo, D. Pisignano, F. Beltram, M. Cecchini, Anal. Chem., 85 (2013) 8080–4.

[25] J.W. Park, B. Vahidi, A.M. Taylor, S.W. Rhee, N.L. Jeon, Nat. Protoc., 1 (2006) 2128–36.

[26] V.N. Goral, C. Zhou, F. Lai, P.K. Yuen, Lab Chip, 13 (2013) 1039–43.

[27] A. Kunze, R. Meissner, S. Brando, P. Renaud, Biotechnol. Bioeng., 108 (2011) 2241–5.

[28] A. Hibara, S. Iwayama, S. Matsuoka, M. Ueno, Y. Kikutani, M. Tokeshi, T. Kitamori, Anal. Chem., 77 (2005) 943–7.

[29] W. Zheng, Z. Wang, W. Zhang, X. Jiang, Lab Chip, 10 (2010) 2906–10.

[30] A.M. Skelley, J. Voldman, Lab Chip, 8 (2008) 1733–7.

[31] C. Lochovsky, S. Yasotharan, A. Günther, Lab Chip, 12 (2012) 595–601.

[32] W. Liu, L. Li, X. Wang, L. Ren, X. Wang, J. Wang, Q. Tu, X. Huang, J. Wang, Lab Chip, (2010) 1717–1724.

[33] R. Gómez-Sjöberg, A. a Leyrat, D.M. Pirone, C.S. Chen, S.R. Quake, Anal. Chem., 79 (2007) 8557–63.

[34] X. Gao, Y. Tanaka, Y. Sugii, K. Mawatari, T. Kitamori, Anal. Sci., 27 (2011) 907.

[35] H.-Y. Wang, N. Bao, C. Lu, Biosens. Bioelectron., 24 (2008) 613–7.

[36] V. Voliani, G. Signore, O. Vittorio, P. Faraci, S. Luin, J. Peréz-Prieto, F. Beltram, J. Mater. Chem. B, 1 (2013) 4225.

[37] N. Korin, A. Bransky, U. Dinnar, S. Levenberg, Lab Chip, 7 (2007) 611–7.

[38] P.J. Hung, P.J. Lee, P. Sabounchi, R. Lin, L.P. Lee, Biotechnol. Bioeng., 89 (2005) 1–8.

[39] S. Petronis, M. Stangegaard, C. Bovöge Christensen, M. Dufva, Biotechniques, 40 (2006) 368–376.

[40] A.B. Das, P. Loying, B. Bose, Cancer Lett., 318 (2012) 189–98.

[41] T.M. Keenan, C.-H. Hsu, A. Folch, Appl. Phys. Lett., 89 (2006) 114103.

[42] A.M. Taylor, M. Blurton-jones, S.W. Rhee, D.H. Cribbs, C.W. Cotman, 2 (2005) 599–605.

[43] J.-M. Peyrin, B. Deleglise, L. Saias, M. Vignes, P. Gougis, S. Magnifico, S. Betuing, M. Pietri,
J. Caboche, P. Vanhoutte, J.-L. Viovy, B. Brugg, Lab Chip, 11 (2011) 3663–3673.

[44] a E. Kamholz, B.H. Weigl, B. a Finlayson, P. Yager, Anal. Chem., 71 (1999) 5340–7.

[45] S. Sugiura, K. Hattori, T. Kanamori, Anal. Chem., 82 (2010) 8278–82.

[46] J.-T. Cao, Y.-D. Zhu, R.K. Rana, J.-J. Zhu, Biosens. Bioelectron., 51 (2014) 97–102.

[47] W.A. El-Said, C.-H. Yea, J.-W. Choi, I.-K. Kwon, Thin Solid Films, 518 (2009) 661–667.

[48] W.A. El-Said, C.-H. Yea, H. Kim, B.-K. Oh, J.-W. Choi, Biosens. Bioelectron., 24 (2009)
1259–65.

[49] H. Bruus, *Theoretical Microfluidics*, Oxford University Press, 2008.

[50] S. Meucci, I. Tonazzini, F. Beltram, M. Cecchini, Soft Matter, 8 (2012) 1109–1119.

[51] I. Tonazzini, S. Meucci, P. Faraci, F. Beltram, M. Cecchini, Biomaterials, 34 (2013) 6027–
6036.

[52] A. Ferrari, M. Cecchini, M. Serresi, P. Faraci, D. Pisignano, F. Beltram, Biomaterials, 31
(2010) 4682–94.

[53] A. Ferrari, M. Cecchini, A. Dhawan, S. Micera, I. Tonazzini, R. Stabile, D. Pisignano, F.
Beltram, Nano Lett., 11 (2011) 505–11.

[54] A. Ferrari, M. Cecchini, R. Degl Innocenti, F. Beltram, IEEE Trans. Biomed. Eng., 56 (2009)
2692–6.

[55] A. Ferrari, P. Faraci, M. Cecchini, F. Beltram, Biomaterials, 31 (2010) 2565–73.

[56] V. Sunkara, D.-K. Park, H. Hwang, R. Chantiwas, S. a. Soper, Y. Cho, Lab Chip, (2011).

[57] P. Gribbon, T.E. Hardingham, Biophys. J., 75 (1998) 1032–9.

[58] M. Rossow, W.W. Mantulin, E. Gratton, J. Biomed. Opt., 14 (2009) 024014.

[59] G. Li, Y. Luo, Q. Chen, L. Liao, J. Zhao, Biomicrofluidics, 6 (2012) 014118.

Figures
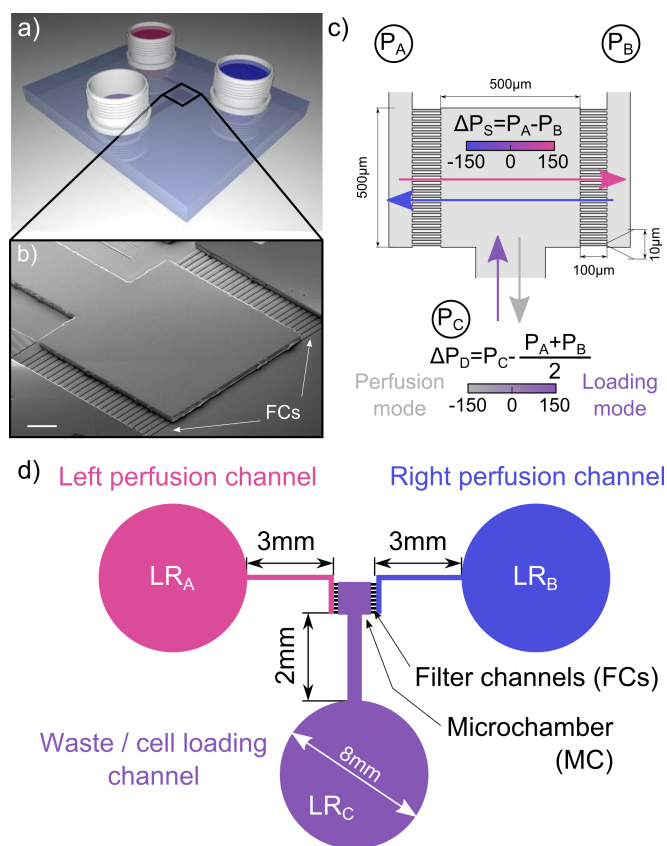
500   Figure 1 Chip design and architecture. a) Schematic model of the device. b) SEM image of the MC

and FCs. Scale bar = 100 μm. c) MC area geometry. The applied pressures (P_A, P_B and P_C) are

indicated inside black circles at the end of the relative channels. The definition of the pressure

differences ΔP_S and ΔP_D is reported and coloured arrows indicate the flow direction in the MC. d)

Architecture of the whole microfluidic network. Different colours identify the three main branches

505   of the device, separated by the FCs.
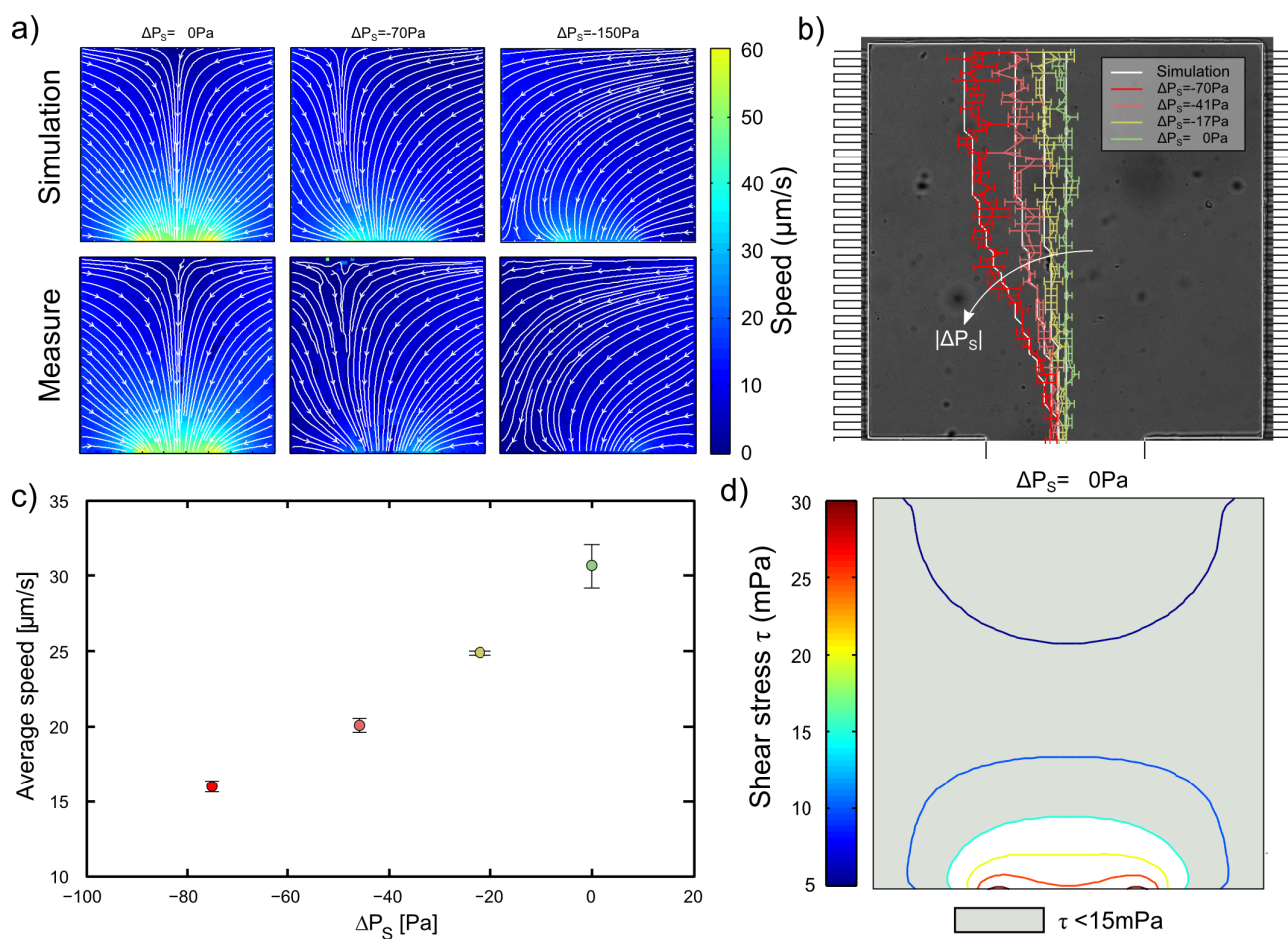
Figure 2 Chip fluid-dynamics characterization. a) Comparison between calculated and experimental velocity fields in the MC. b) Unbalanced flow in the MC: the position of the interface between fluid flows from the PCs is calculated (solid line) and measured (coloured bars) for different values of ΔP_S. The average speed of each pressure configuration is plotted in (c). d) Map of the shear stress in the MC during symmetric perfusion ($\Delta P_D = 150$ Pa, $\Delta P_S = 0$ Pa).
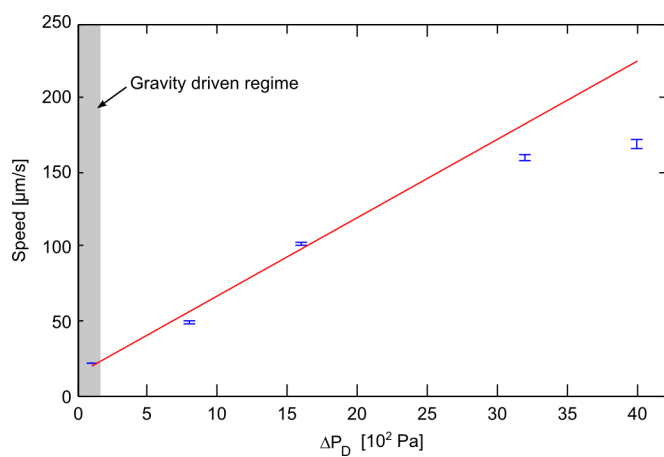
Figure 3 Measure of speed (blue dots) in the MC during active pressurization. A linear fit of the

515   first three points (pure resistive regime) of the curve (red line) is reported (see Sec 3.1 for detail).

26
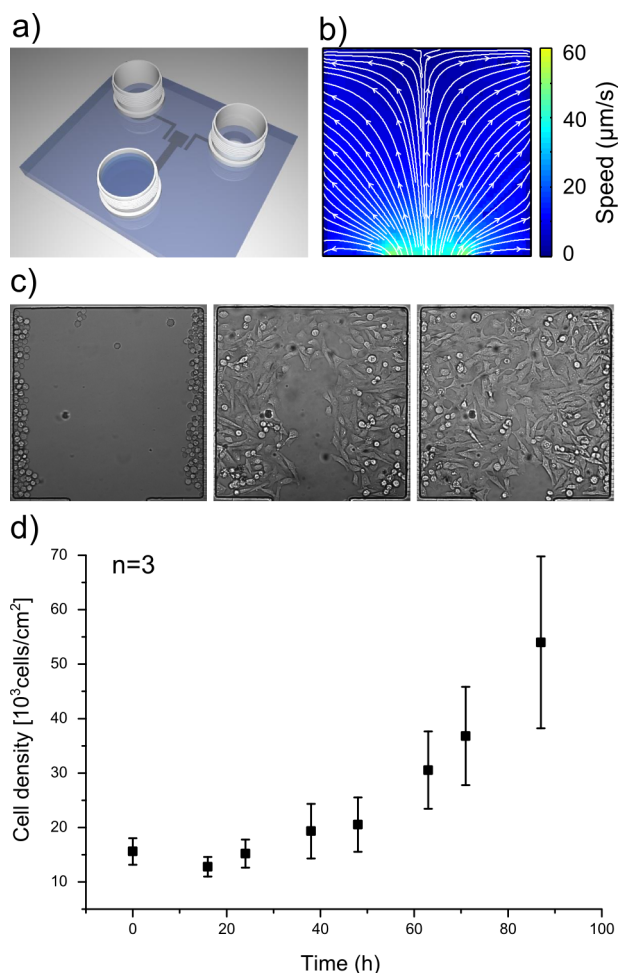
Figure 4: Cell loading and chip cytocompatibility. a) Scheme of the chip configuration during cell loading. Liquid is removed from LR_A and LR_B, and the cell suspension is added in the LR_C. b) Measure of the velocity field during cell loading ($\Delta P_D = -150$ Pa, $\Delta P_S = 0$ Pa). c) Time lapse images showing HeLa cells loading and chamber colonization. d) Measure of the HeLa cell density as a function of time during long-term cell culture ($\Delta P_D = 150$ Pa, $\Delta P_S = 0$ Pa).
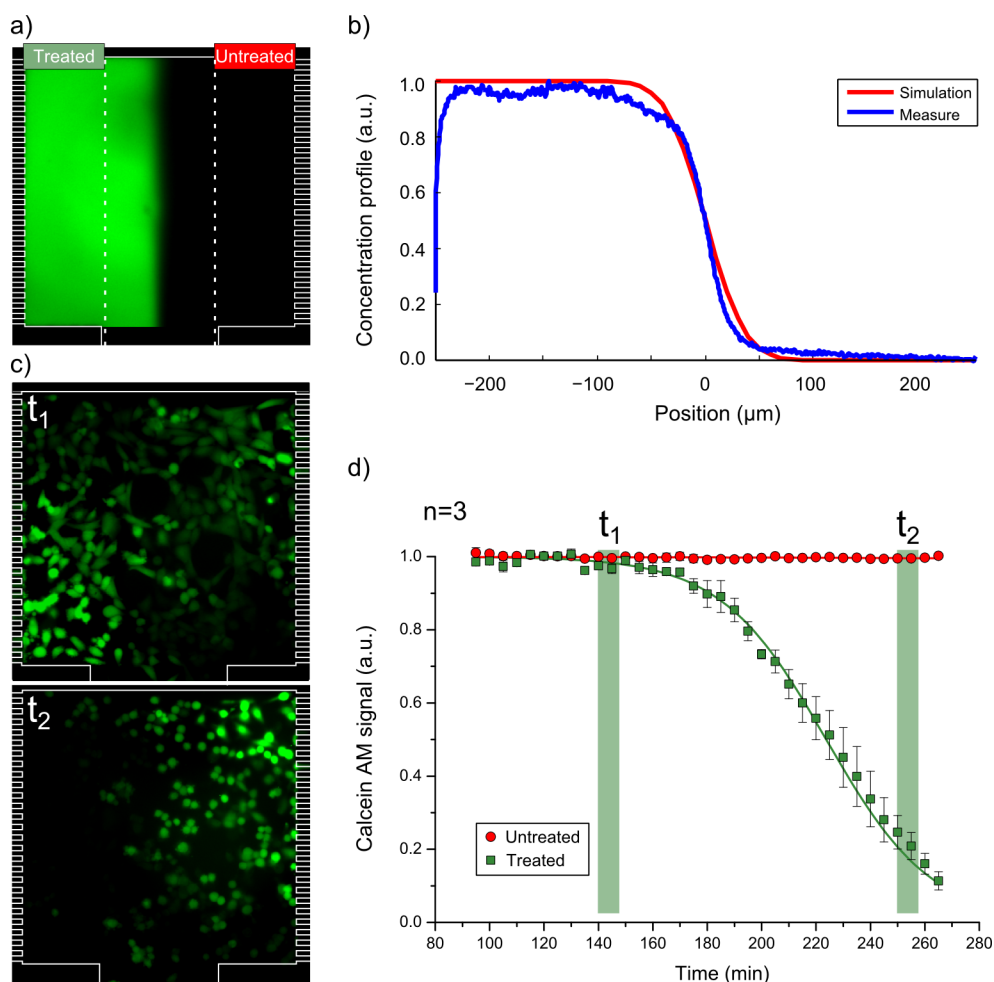
Figure 5: CT-Dex-induced cell-death. a) Visualization of a stable Fluorescein-Dex gradient in the

525   MC ($\Delta P_D = 150$ Pa, $\Delta P_S = 0$ Pa). Dashed lines identify two regions of the MC (treated and untreated) where the drug concentration is considered constant (high and low, respectively). b) Comparison between theoretical and experimental gradient profiles. c) Calcein AM fluorescensce at different times during CT-Dex treatment. d) Quantification of the Calcein AM signal during CT-Dex local administration measured by time-lapse fluorescence microscopy. Green and red curves

530   are the normalized integral of the fluorescence signal in treated and untreated regions, respectively. The signal was normalized to take photobleaching into account.

Supplementary material

For TOC only